Reaction Kinetics, Mechanisms and Catalysis (2023) 136:233–250
https://doi.org/10.1007/s11144-022-02336-1

Sol–gel prepared Co–Mg–O oxide systems: redox behavior, thermal stability and catalytic performance in CO oxidation

Grigory B. Veselov[1] · Vladimir O. Stoyanovskii[1] · Svetlana V. Cherepanova[1] · Aleksey A. Vedyagin[1]

Received: 12 October 2022 / Accepted: 13 December 2022 / Published online: 18 December 2022
© Akadémiai Kiadó, Budapest, Hungary 2022

Abstract

In this work, Co–Mg–O oxide systems were prepared via a sol–gel technique. The cobalt loading in the samples was varied from 1 to 45 wt% (in relation to Co_3O_4). During the synthesis, magnesium methoxide was hydrolyzed by an aqueous solution of cobalt nitrate of corresponding concentration. The desired pH value of the solution was set by the addition of ammonia or nitric acid. The decomposition of xerogel was examined using thermogravimetric method. The prepared Co–Mg–O oxide samples were characterized by low-temperature nitrogen adsorption, X-ray diffraction analysis, and diffuse reflectance UV–vis spectroscopy. Finally, the samples were tested in consecutive redox cycles (temperature-programmed reduction in hydrogen followed by reoxidation in air) and in a model reaction of carbon monoxide oxidation studied under prompt thermal aging conditions. As found, in the case of as-prepared samples, cobalt interacts with MgO with the formation of such a solid solution as $MgCo_2O_4$. With an increase in the Co_3O_4 loading, this interaction becomes stronger. Each reduction/oxidation cycle leads to an emergence of a part of cobalt from the solid solution, thus increasing the amount of isolated Co_3O_4 particles distributed within the MgO matrix. The sample prepared with the ammonia addition exhibited the highest stability in catalytic runs if compared with other samples. An increase in Co_3O_4 loading from 5 to 30% decreases the light-off temperature in first runs but affects negatively the thermal stability.

✉ Aleksey A. Vedyagin
vedyagin@catalysis.ru

[1] Boreskov Institute of Catalysis, Novosibirsk, Russia

Graphical abstract

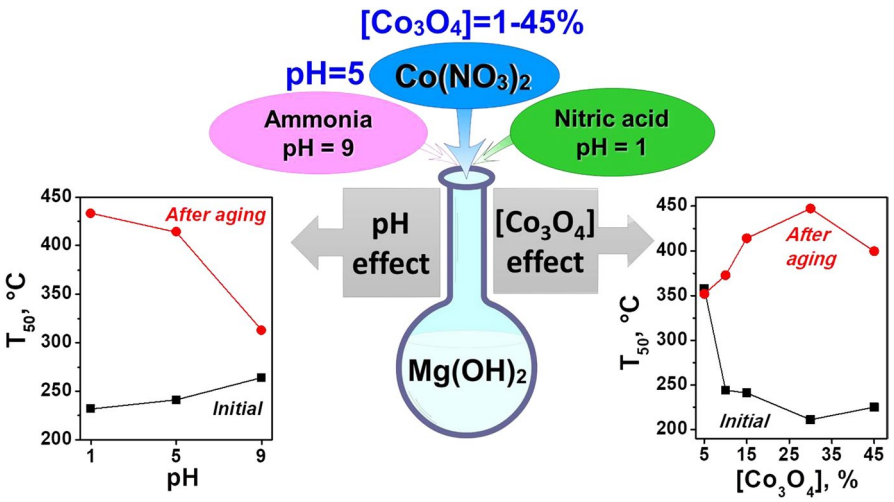

Keywords Sol–gel synthesis · Co-based systems · MgO matrix · Reducibility degree · CO oxidation

Introduction

Because of its redox properties, cobalt oxide is highly demanded for various electrochemical and catalytic applications [1–10]. In particular, supported Co_3O_4 catalysts are proven to be highly active in a number of oxidation processes, including oxidation of carbon monoxide and hydrocarbons. Since the smaller size of the active component particles corresponds to the higher catalytic activity, various materials have been checked for the stabilization of the dispersed cobalt oxide species. For instance, the choice of the support (CeO_2, ZrO_2, SiC, SiO_2 and Al_2O_3) has been shown to affect the performance of Co_3O_4 nanoparticles in the preferential CO oxidation in an H_2-rich environment [5]. Thus, the strength of the cobalt oxide-support interaction defines the oxidation state of cobalt and, consequently, its catalytic activity. In the case of weak interaction, like for ZrO_2, the catalyst shows high activity. Oppositely, a strong interaction of Co_3O_4 with Al_2O_3 leads to the suppression of the Co^0 state and the formation of methane. Another system, Co_3O_4 supported on Ni foam prepared by an electro-deposition, demonstrates higher specific activity and lower activation energy in propane oxidation, in comparison with unsupported Co_3O_4, and retained its catalytic activity for 40 h on stream [6]. Zhu et al. [9] have reported that Co_3O_4 nanoparticles supported on activated carbon exhibited ~ 100% conversion in benzylic alcohol oxidation to benzaldehyde. Tang et al. [10] have studied the CO oxidation reaction and found that monolithic Co_3O_4/TiO_2 catalysts appeared able to oxidize CO completely at 120 °C, demonstrating excellent stability.

The MgO-based cobalt-containing systems also attract attention of the researchers. They are applied as catalysts for a variety of redox reactions such as decomposition of N_2O [11–14], reforming of naphthalene [15], dehydrogenation of ethanol [16], cyclohexane oxidation with molecular oxygen [17], CO oxidation [18], hydrogen peroxide decomposition [18, 19], etc. $MgCo_2O_4$ spinel is attractive to be used as cathode materials [20–23] and supercapacitors [24, 25].

In the case of Co_3O_4-MgO oxide systems, an interaction between Co_3O_4 and MgO can lead to the formation of two types of solid solutions: $Co_xMg_{1-x}O$, formed by the substitution of Mg^{2+} ions in MgO lattice with Co^{2+}; and $Mg_xCo_{3-x}O_4$, where Mg^{2+} ions can be located in both tetrahedral and octahedral positions [26]. The fraction of cobalt oxide dissolved in MgO increases with the calcination temperature, and the complete formation of $Co_xMg_{1-x}O$ phase takes place at 1000 °C. No spinel phase is present in this case [15, 27]. Mg^{2+} ions can be intercalated into the $MgCo_2O_4$ structure with the formation of $Mg_2Co_2O_4$ rock salt phase, which opens a possibility for $MgCo_2O_4$ to be used as a positive electrode in magnesium rechargeable batteries [22, 28].

The method of temperature-programmed reduction with hydrogen (TPR-H_2) is informative and helpful in examination of phase composition of the Co_3O_4-MgO systems. The reduction of bulk Co_3O_4 occurs in a temperature range of 300–500 °C via two steps: $Co_3O_4 \rightarrow CoO$ (1), and $CoO \rightarrow Co^0$ (2) [29]. These stages begin at similar temperatures and, therefore, in the TPR-H_2 profiles, a peak assigned to the step (1) appears as a left shoulder. However, in the case of Co_3O_4 nanoparticles, including supported ones, these two peaks are often separated [30].

As it was reported by Sadasivan et al. [31], the particle size of the Co_3O_4 particles significantly affects their behavior in reduction–oxidation–reduction experiments. The reduction stage proceeds relatively easily. Contrary, re-oxidation of large Co particles is constrained. This stage results in the formation of a core–shell structure with a thickness of cobalt oxide layer of ~ 3 nm. Complete oxidation of cobalt requires higher temperatures and leads to the formation of hollow Co_3O_4 spheres. Reduction of such spheres results in their fragmentation and appearance of smaller metallic cobalt particles.

The reduction of the Co_3O_4-MgO systems often proceeds through the multiple stages [15, 30]. In this case, the stages (1) and (2) usually occur at ~ 340 °C and ~ 500 °C, respectively. Hydrogen uptake due to reduction of the $MgCo_2O_4$ and $Co_xMg_{1-x}O$ phases is registered in a wide temperature range with maxima at ~ 700 °C and ~ 1000 °C. At the same time, the introduction of MgO in Co_3O_4/Al_2O_3 systems leads to a shift of the Co_3O_4 reduction range to lower temperatures despite the formation of $Mg_xCo_{3-x}O_4$ spinel [11, 14]. As reported, the catalytic activity in N_2O decomposition is higher for samples that contain MgO. Partial substitution of Co^{2+} in Co_3O_4 with Mg^{2+} weakens Co–O bonds and, therefore, increases the activity. Similar effects were shown for the supported Co_3O_4–containing catalysts of methane combustion [32]. In this case, the reaction rate evidently correlates with the hydrogen uptake in TPR-H_2 experiments.

It should be noted that cobalt oxide is also considered as an oxygen carrier for chemical looping processes but there are only a few works addressed to this topic. Despite its favorable thermodynamics in oxidation processes, relatively high

resistance to sintering and coking, the high toxicity and cost of cobalt compounds and the low decomposition temperature of cobalt oxide (Co_3O_4) are the major concerns [33–35]. Since the solid–solid interactions in Co_3O_4–MgO systems can lead to the phases with improved thermal stability, their application as oxygen carriers is of particular interest.

Previously, an alkoxide sol–gel method was successfully used to prepare a set of MgO-based systems [36–39]. In the present work, the same technique was utilized to prepare a series of Co–Mg–O samples. Both the concentration of cobalt nitrate and the pH of solution used for the hydrolysis of magnesium methoxide were varied. The resulting xerogels and oxides were characterized by such physicochemical methods as differential thermal analysis (DTA), low-temperature nitrogen adsorption, X-ray diffraction (XRD), and UV–Vis diffuse reflectance (DRS) spectroscopy. Redox behavior of the samples was studied by the method of temperature-programmed reduction in hydrogen atmosphere (TPR-H_2). A model reaction of CO oxidation performed under prompt thermal aging conditions was chosen to compare the catalytic performance and the thermal stability of the samples.

Experimental

Preparation of the samples

The Co–Mg–O oxide systems were prepared via a sol–gel route as described elsewhere [40]. At first, magnesium ribbon was dissolved in methanol, thus forming a magnesium methoxide solution. For each 1 g of magnesium, 43 mL of methanol was used. As shown previously [41], the addition of toluene during the synthesis of magnesium hydroxide significantly improves its textural properties. Therefore, toluene was added to the solution of magnesium methoxide in a volumetric ratio of 1:1 with regard to methanol. The hydrolysis of magnesium methoxide was performed using an aqueous solution of cobalt nitrate, which was added dropwise. Thus, a viscous gel has been formed. The gel was dried at room temperature for 2 h and at 200 °C for another 2 h. The resulting xerogels were heated with a ramping rate of 1 °C/min up to 500 °C and calcined at this temperature for 1 h.

During this study, the effects of cobalt content and pH of the solution at the hydrolysis stage were examined. With this regard, the concentration of cobalt nitrate in the aqueous solution on the hydrolysis stage was appropriately varied. Thus, 0.067, 0.316, 0.668, 1.060, 2.575, or 4.915 g of $Co(NO_3)_2{\cdot}6H_2O$ were dissolved in 3 mL of distilled water to obtain the cobalt loading (in relation to Co_3O_4) of 1, 5, 10, 15, 30, or 45 wt%, correspondingly. Note that pH of this solution is equal to 5. In order to vary the pH values, nitric acid or ammonia were added into the cobalt nitrate solution. Thus, the addition of nitric acid and ammonia resulted in pH 1 and 9, correspondingly. The prepared samples were labeled as X%Co–Mg–O(Y), where X is the Co_3O_4 content and Y is the pH value.

The reference sample of bulk Co_3O_4 was obtained by calcining the $Co(NO_3)_2 \times 6H_2O$ precursor. In order to exclude any effects of preparation

procedures, the reference sample was subjected to the same thermal treatment as the Co–Mg–O samples.

Characterization of the samples

Low-temperature nitrogen adsorption technique was used to obtain the textural characteristics of the Co–Mg–O samples (specific surface area, SSA; pore volume, V_{pore}; average pore diameter, D_{av}). Note that the average pore diameter was calculated using a simple cylindrical model. The nitrogen adsorption/desorption isotherms were recorded at 77 K using an ASAP-2400 (Micromeritics, Norcross, GA, USA) instrument.

Powder X-ray diffraction (XRD) analysis of the Co–Mg–O samples was carried out using an X'TRA (Thermo ARL, Ecublens, Switzerland) diffractometer with Cu K_α radiation source. The patterns were recorded in a 2θ angle range of 15°–85° with accumulation time in each point of 5 s. Average crystallite sizes were calculated using TOPAS software (Bruker, Billerica, MA, USA).

Diffuse reflectance UV–vis spectra of the samples were recorded between 190 and 800 nm using a UV–vis spectrometer Varian Cary 300 UV/VIS Bio (Agilent Technologies, Palo Alto, CA, USA) with a IRS-250A diffusion refection attachment and a DRA-CA-3300 integrating sphere (Labsphere, North Sutton, NH, USA). The spectra were transformed into the Kubelka–Munk function $F(R) = (1-R)^2/2R$, where R is the experimentally measured reflectivity coefficient of the samples [42].

The reduction/oxidation behavior of the samples was studied by means of temperature-programmed reduction in a hydrogen atmosphere (TPR-H_2). The specimen (200 mg) was loaded into a quartz reactor and kept in a nitrogen flow at 30 °C for 30 min. Then, the reactor was fed with a mixture of 10 vol% H_2 in N_2. The total flow rate was 57.8 mL/min. The reactor was heated up to 700 °C with a ramping rate of 10 °C/min and maintained at this temperature for 15 min. The outlet hydrogen concentration was measured using a gas analyzer GAMMA-100 (Analitpribor, Smolensk, Russia) equipped with a thermal conductivity detector. Then, the reactor was cooled down to 30 °C. For the re-oxidation of the sample, the reactor was fed with a flow of air diluted with nitrogen in a ratio of 2:1 (10 mL/min of air, 5 mL/min of N_2), heated up to 500 °C at a ramping rate of 20 °C/min, maintained at the final temperature for 30 min and cooled down to 30 °C. Such a reduction/oxidation cycle was repeated seven times. The reference sample of bulk Co_3O_4 was examined using the described TPR-H_2 technique in five cycles. In this case, the specimen was 100 mg. The reducibility values were calculated using the following equation:

$$\text{Reducibility (\%)} = \text{Total hydrogen uptake (mmol/g)/Theoretical uptake (mmol/g)} \times 100\%,$$

Here *theoretical uptake* is a value calculated assuming that all the CoO_x species are in the form of Co_3O_4. Therefore, the reducibility can exceed 100% if an excess of the Co^{3+} species is present. Note that the measurement uncertainty of this method was ± 3%.

The catalytic performance of the samples was investigated in a model reaction of CO oxidation. The experiments were carried out under prompt thermal aging conditions, which allowed monitoring the thermal stability as well [43, 44]. The specimen (300 mg, fraction of 0.25–0.5 mm) was loaded into a quartz flow-through reactor. The reactor was fed with a reaction mixture containing 0.15 vol% CO, 14.0 vol% oxygen, and balance nitrogen with a flow rate of 334 mL/min. In each catalytic cycle, the reactor was heated from 50 °C to the final temperature with a ramping rate of 10 °C/min. The final temperature was varied in cycles and corresponded to 320 °C (cycles 1 and 2), 600 °C (cycles 3 and 4), 800 °C (cycles 5 and 6), 900 °C (cycles 7 and 8), 1000 °C (cycles 9 and 10), and 500 °C (cycle 11). CO concentration was monitored every two seconds using a gas analyzer ULTRAMAT 6 (Siemens AG, Karlsruhe, Germany). The temperature of 50% CO conversion (T_{50}) was used as a criterion to compare the samples.

Results and discussions

It is well known that processes occurring during the thermal treatment procedures can significantly affect the porous structure and the textural characteristics of well-dispersed materials. In order to study the thermal decomposition of the Co–Mg–OH xerogels, the samples were collected after drying at 200 °C. The results of the thermogravimetric measurements are presented in the Supplementary Information.

Textural characteristics and phase composition of the samples

Such characteristics as specific surface area (SSA), pore volume (V_{pore}), and average pore diameter (D_{av}) of the samples were examined by low-temperature nitrogen adsorption/desorption. Table 1 summarizes these data. Comparing the samples

Table 1 Textural characteristics of the studied Co–Mg–O samples

Sample	Co_3O_4 content, %	pH	SSA, m^2/g	V_{pore}, cm^3/g	D_{av}, nm
1%Co–Mg–O(5)	1	5	233	0.77	13
5%Co–Mg–O(5)	5	5	177	0.81	18
15%Co–Mg–O(1)	15	1	119	1.31	44
15%Co–Mg–O(5)*	15	5	165	0.88	21
15%Co–Mg–O(9)	15	9	71	0.63	36
30%Co–Mg–O(5)	30	5	147	0.63	17
45%Co–Mg–O(5)	45	5	120	0.56	19
15%Co–Mg–O(5)r**	15	5	57	0.18	12
30%Co–Mg–O(5)r**	30	5	35	0.15	17
45%Co–Mg–O(5)r**	45	5	27	0.16	24

*These data are taken from recently reported paper [36]; **The samples labeled by "r" are after the TPR-H_2 experiments

prepared at different pH, it can be seen that the total pore volume decreases in a row: 15%Co–Mg–O(1) > 15%Co–Mg–O(5) > 15%Co–Mg–O(9). At the same time, the 15%Co–Mg–O(5) sample possesses the highest SSA value among this series (165 m^2/g). The observed tendencies can be explained by the difference in ionic strength during the gel formation stage as well as by the pH effect on the hydrolysis and polymerization rates. Thus, the polymerization rate is higher at the higher pH values. This leads to the formation of larger sol particles and appearance of larger MgO particles after the calcination stage [45]. The local temperature increase due to the previously mentioned exothermic effect also facilitates an enlargement of the xerogel particles being formed.

The effect of the Co_3O_4 loading on the textural characteristics is also well seen from Table 1. The SSA value decreases in the following order: 1%Co–Mg–O(5) > 5%Co–Mg–O(5) > 15%Co–Mg–O(5) > 30%Co–Mg–O(5) > 45%Co–Mg–O(5). The total pore volume shows a volcano-shaped dependence with a maximum at 15% of Co_3O_4. It can be assumed that an increase in the ionic strength of the solution at the hydrolysis stage reduces the stability of the magnesium hydroxide sol, thus leading to a rapid particle aggregation. As a result, the particles grow in size, and the pore radius increases accordingly.

The X-ray diffraction patterns for the samples obtained at varied pH are shown in Fig. 1. Note that the detailed XRD data for the 15%Co–Mg–O(5) sample were reported recently [36, 40]. All the patterns are represented by the reflections attributed to MgO phase and cobalt oxide Co_3O_4. The results of the XRD analysis are presented in Table 2. It should be noted that the lattice parameter of MgO is increased in comparison with the literature value of 4.211 Å (PDF#45-0946). The similar phenomenon was earlier reported for the MgO-based systems [36]. Since the lattice

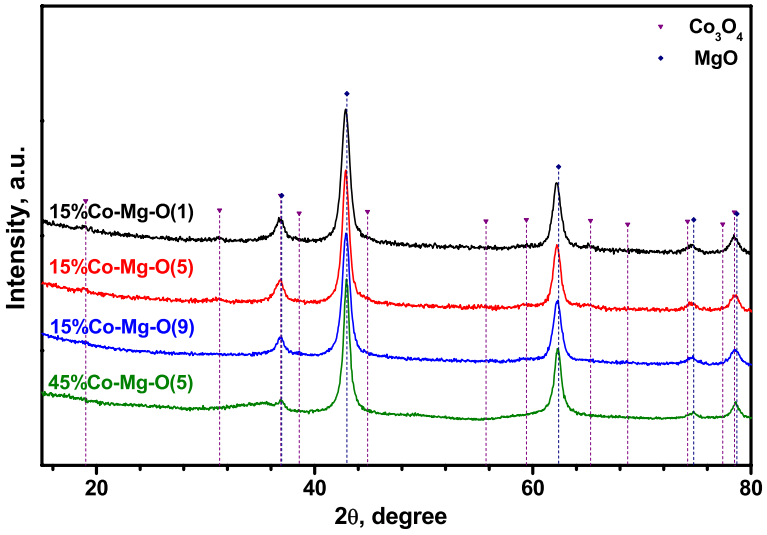

Fig. 1 XRD patterns for the 15%Co–Mg–O samples obtained at various pH and for the 45%Co–Mg–O(5) sample

Table 2 Quantitative results of XRD analysis for the 15%Co–Mg–O samples obtained at various pH

Sample	MgO phase		Co_3O_4 phase		
	a (Å)	D (nm)	Estimated content (wt%)	a (Å)	D (nm)
15%Co–Mg–O(1)	4.221(1)	8	6	8.13	4.0
15%Co–Mg–O(5)	4.219(1)	9	6	8.13	5.5
15%Co–Mg–O(9)	4.220(1)	8	7	8.12	2.5

parameter of CoO (a = 4.26 Å, PDF#43-1004) is higher than the lattice parameter of MgO, this shift can also be explained by the substitution of Mg^{2+} ions with Co^{2+} ions in the magnesium oxide lattice. The lattice parameter of Co_3O_4 (a = 8.083 Å, PDF#42-1467) is also shifted. It is close to the value expected for $MgCo_2O_4$ (a = 8.123 Å, PDF#02-1073). Thereby, the formation of the $Mg_xCo_{3-x}O_4$ solid solutions is confirmed by the XRD data. The crystallite size of the particles depends on the pH value at the hydrolysis stage (Table 2). The largest crystallites (5.5 nm) are observed in case of the 15%Co–Mg–O(5) sample. When ammonia or HNO_3 are added, the particles are noticeably smaller in size. It is important to note that no intensive reflexes related to the Co_3O_4 phase can be found even in the case of the 45%Co–Mg–O(5) sample containing the highest amount of cobalt. This allows suggesting that the higher amount of Co_3O_4 does not lead to the formation of an odd amount of the spinel-type phase. The excess cobalt dissolves in the MgO matrix and participates in the formation of $Mg_{1-x}Co_xO$ solid solutions. Such a supposition correlates with the TPR-H_2 data presented later on.

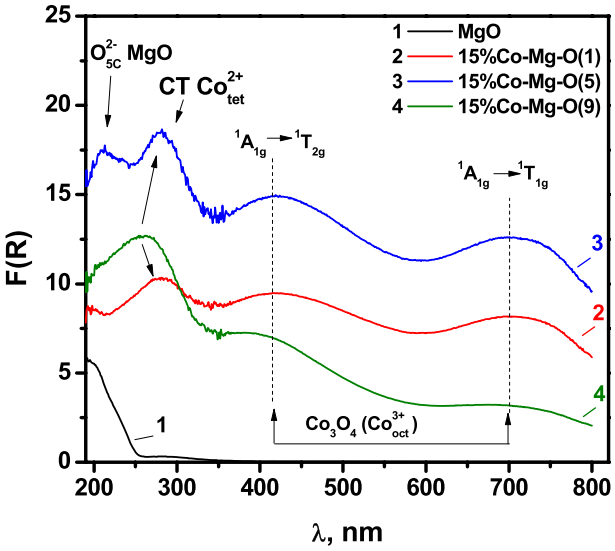

Fig. 2 Diffuse reflectance UV–vis spectra of the 15%Co–Mg–O samples prepared at different pH

Fig. 2 demonstrates the diffuse reflectance UV–vis spectra of pure MgO and the samples 15%Co–Mg–O(1), 15%Co–Mg–O(5), and 15%Co–Mg–O(9). The absorption spectra, excluding the band at 190–220 nm corresponding to O^{2-} over the MgO surface (surface five-fold coordinated anions, 6.6 eV; O^{2-} surface four-fold coordinated anions on the edge, 5.6 eV), are defined by cobalt. They are characterized by the two intensive bands at 415 and 700 nm, corresponding to the transitions $^1A_{1g} \rightarrow {}^1T_{2g}$ and $^1A_{1g} \rightarrow {}^1T_{1g}$ of Co^{3+} in octahedral positions of the Co_3O_4 spinel particles [46–48]. The band of the charge transition between oxygen ligands and Co^{2+} in tetrahedral symmetry at 270 nm is typical for spinel-type oxides like $MgCo_xAl_{2-x}O_4$ [48, 49] and $Mg_xCo_{3-x}O_4$ [30, 50]. Note that this band is absent in the case of Co_3O_4, and its appearance in spectra confirms the presence of $MgCo_2O_4$, which is consistent with the XRD data.

As follows from the presented spectra (Fig. 2), the intensities of the bands $^1A_{1g} \rightarrow {}^1T_{2g}$ and $^1A_{1g} \rightarrow {}^1T_{1g}$ of Co^{3+} increase in a row: 15%Co–Mg–O(9) < 15%Co–Mg–O(1) < 15%Co–Mg–O(5). Such an increase in the band intensity for the nanosized particles at similar cobalt concentration can be attributed to the enlargement of the particles. This assumption correlates well with the XRD data. The charge transition band is shifted towards the region of long wavelengths that can also be connected with the size effects (the energy-gap width decreases with the particle size increase). The intensities of the four-fold and five-fold coordinated O^{2-} anions over the MgO surface decreases in a row: 15%Co–Mg–O(5) > 15%Co–Mg–O(9) > 15%Co–Mg–O(1), thus approaching to that for pure MgO. This denotes the possible differences in morphology or size of MgO particles within the studied series.

Study on reducibility and redox behavior of the samples

The reduction behavior of the samples was studied using the method of temperature-programmed reduction in hydrogen (TPR-H_2). Firstly, the reference sample of bulk Co_3O_4 was studied. The TPR-H_2 profiles for five consecutive cycles are presented in Fig. 3. The reduction of the fresh sample takes place in a wide temperature range from 200 to 450 °C. The profile has one maximum at 400 °C and two shoulders at 295 and 355 °C. The appearance of the low-temperature shoulder can be attributed to the reduction of the smaller Co_3O_4 particles or the surface oxygen species. Then, Co_3O_4 reduces via the two-stage process [29]. The calculated hydrogen uptake corresponds to the value expected for the stoichiometric phase Co_3O_4, and the reducibility degree is equal to 100%. Starting from the second cycle, the reducibility degree rapidly falls down, reaching 15.5% in the fifth cycle. Such a behavior is evidently connected with the sintering of cobalt oxide particles.

The cobalt-containing MgO-based systems behave in a different manner. The corresponding TPR-H_2 profiles are shown in Fig. 4.

In the case of the 15%Co–Mg–O(1) sample (Fig. 4a), there are few peaks, which can be attributed to the different states of cobalt. The low-temperature peak at 180 °C corresponds to the reduction of oxygen species over the surface of dispersed Co_3O_4 particles [30]. The next two peaks at 285 and 465 °C seem to be the stages

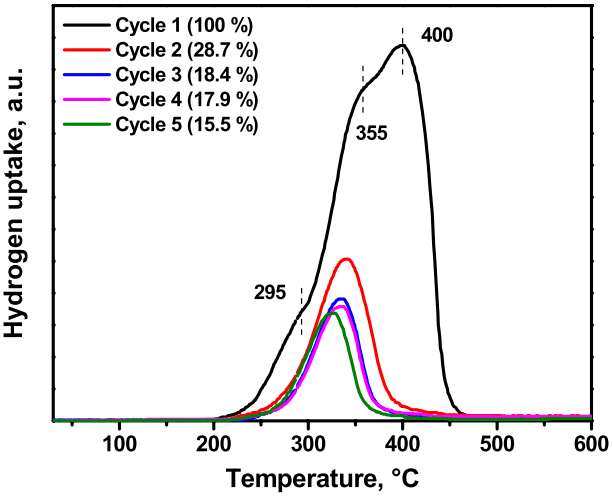

Fig. 3 TPR-H_2 profiles and reducibility degree values in five consecutive redox cycles for bulk Co_3O_4 (reference sample)

$Co_3O_4 \rightarrow CoO$ and $CoO \rightarrow Co$, correspondingly [29]. These peaks are evidently separated on the temperature scale that is typical for supported cobalt oxide. The peak at ~ 680 °C can be assigned to the reduction of $MgCo_2O_4$ spinel. As calculated (Table 3), the total hydrogen uptake reaches 87.7% of the theoretical value. This testifies towards the presence of other cobalt species in the samples, which require higher temperatures to be reduced. For instance, solid solution $Co_xMg_{1-x}O$ does not reduce under such conditions. In the subsequent cycles, a shift of the peaks towards the low-temperature region is observed. Such a behavior can be supposedly explained by the weakening of cobalt interaction with the MgO matrix during the TPR-H_2 experiments. At the same time, the reducibility degree in the last cycle achieved 92.3%.

The reduction behavior of the 15%Co–Mg–O(5) sample prepared without addition of ammonia or nitric acid is similar to that described above (Fig. 4b). The positions of the hydrogen uptake peaks coincide within 10–15 °C. However, the higher values of reducibility degree are well seen (Table 3).

The highest total hydrogen uptake value in the first cycle was demonstrated by the 15%Co–Mg–O(9) sample (Table 3). As known, ammoniac complexes of cobalt (II) can be easily oxidized in air to complexes of cobalt (III). Thereby, this sample can supposedly contain a higher amount of Co^{3+} species. The changed shape of the peak at 290 °C indirectly confirms this supposition. In the subsequent cycles, the positions of the peaks remained practically the same but their intensities changed. As shown by the XRD and UV–vis techniques, the Co_3O_4 particles in this sample are of the smallest size. Therefore, their sintering is complicated due to stronger interaction with the MgO matrix. For instance, Moogi et al. have reported [51] that the smaller Co_3O_4 particles in Co_3O_4-based catalysts are less prone to sintering if compared to the larger ones. Indeed, the reducibility degree in the seventh cycle (78.0%)

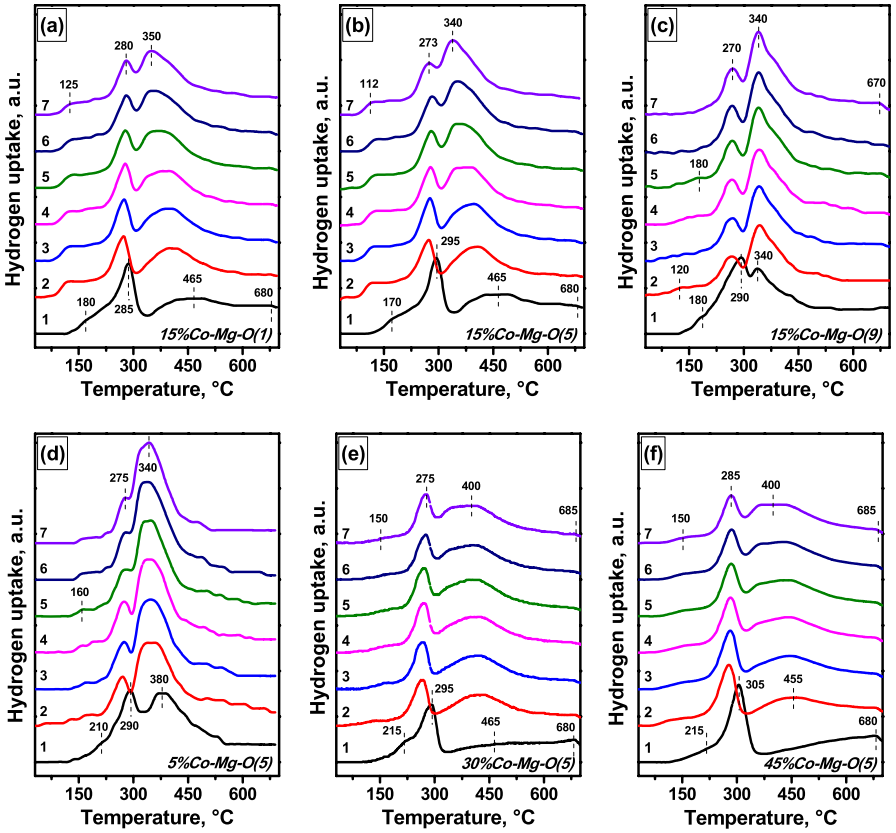

Fig. 4 TPR-H_2 profiles for the studied samples: **a** 15%Co–Mg–O(1); **b** 15%Co–MgO(5); **c** 15%Co–Mg–O(9); **d** 5%Co–Mg–O(5); **e** 30%Co–Mg–O(5); **f** 45%Co–Mg–O(5). The hydrogen uptake intensity is normalized to cobalt content. The number of cycle is written above each curve

Table 3 Reducibility degree of the Co–Mg–O samples in the first and seventh TPR-H_2 cycles

Sample	Reducibility degree (%)	
	First cycle	Last cycle
5%Co–Mg–O(5)	99.6	85.4
15%Co–Mg–O(1)	87.7	92.3
15%Co–Mg–O(5)	93.7	96.6
15%Co–Mg–O(9)	104	78.0
30%Co–Mg–O(5)	57.1	62.5
45%Co–Mg–O(5)	61.9	70.4

is noticeably lower if compared with the 15%Co–Mg–O(1) and 15%Co–Mg–O(5) samples (Table 3). Moreover, the additional peak at 670 °C has appeared.

In order to analyze the effect of the cobalt loading on the reduction behavior, the profiles shown in Fig. 4b–f should be compared. The TPR-H_2 profiles for the

5%Co–Mg–O(5) sample (Fig. 4d) resemble the data for the 15%Co–Mg–O(9) sample. Such a similarity in the reduction behavior can be explained by a relatively close size of the Co_3O_4 particles in these samples. In the first cycle, the two peaks at 290 and 340 °C correspond to the two-stage reduction of Co_3O_4 to CoO. Then, from cycle to cycle, the intensity of the first peak decreases along with the increase in contribution of the second peak. During the experiments, cobalt partly transforms into the hardly-reducible species, and the reducibility degree falls from 99.6 to 85.4%.

An opposite situation is observed for the high-loaded samples 30%Co–Mg–O(5) and 45%Co–Mg–O(5). There is an increase in the contribution of cobalt in the form of $MgCo_2O_4$, which reduction occurs at ~ 670 °C (Fig. 4e, f). The lower values of the reducibility degree (Table 3) testify towards the formation of a solid solution $Co_xMg_{1-x}O$. As in case of the 15%Co–Mg–O(5) sample, part of cobalt leaves these solid solutions after the first cycle of reduction/oxidation. In subsequent cycles, the hydrogen uptake peaks assigned to the reduction of Co_3O_4 and CoO have appeared at ~ 280 °C and ~ 400 °C, accordingly. Contrary to the 15%Co–Mg–O(5) sample, for these two samples, the low-temperature hydrogen uptake (at ~ 150 °C), corresponding to the reduction of surface oxygen on the Co_3O_4 species, is significantly lower. Thereby, a worse dispersity of the Co_3O_4 particles can be assumed. The cyclic reduction/oxidation of cobalt species leads to the redispersion of coarse particles, and an increase in the reducibility degree is observed for these samples.

The samples 15%Co–Mg–O(5), 30%Co–Mg–O(5), and 45%Co–Mg–O(5) after the seven redox cycles were additionally characterized by low-temperature nitrogen adsorption (Table 1). As seen, all the textural characteristics changed significantly. Thus, the SSA values decreased in 3–3.5 times, while the total pore volume diminished in 4–5 times. For the average pore size, an inverse relationship is observed. In the case of 15%Co–Mg–O(5), the D_{av} decreased from 21 to 12 nm. No changes happened with the 30%Co–Mg–O(5) sample. And for the 45%Co–Mg–O(5) sample, the D_{av} increased from 19 to 24 nm. All these observations can be explained by the high-temperature processes leading to the enlargement of MgO crystallites along with Co-containing species.

Catalytic performance in CO oxidation under promt thermal aging conditions

The catalytic performance of the Co–Mg–O samples was studied in a model reaction of CO oxidation. The catalytic tests were performed under prompt thermal aging (PTA) conditions, when the final temperature after each second catalytic cycle was increased. The final temperature values were as follows: 320 °C; 600 °C; 800 °C; 900 °C; 1000 °C. The use of the PTA approach allows monitoring the thermal stability as well. The typical light-off curves are shown in Fig. 5a. The temperature of 50% CO conversion (T_{50}) was used as a criterion. As seen, each change of the final temperature affects the position of the light-off curve, thus indicating deactivation (when T_{50} increased) or reactivation (when T_{50} decreased) of the active species.

Fig. 5b, c present the T_{50} values depending on the number of catalytic cycle. The samples prepared at various pH are compared in Fig. 5b. In general, the

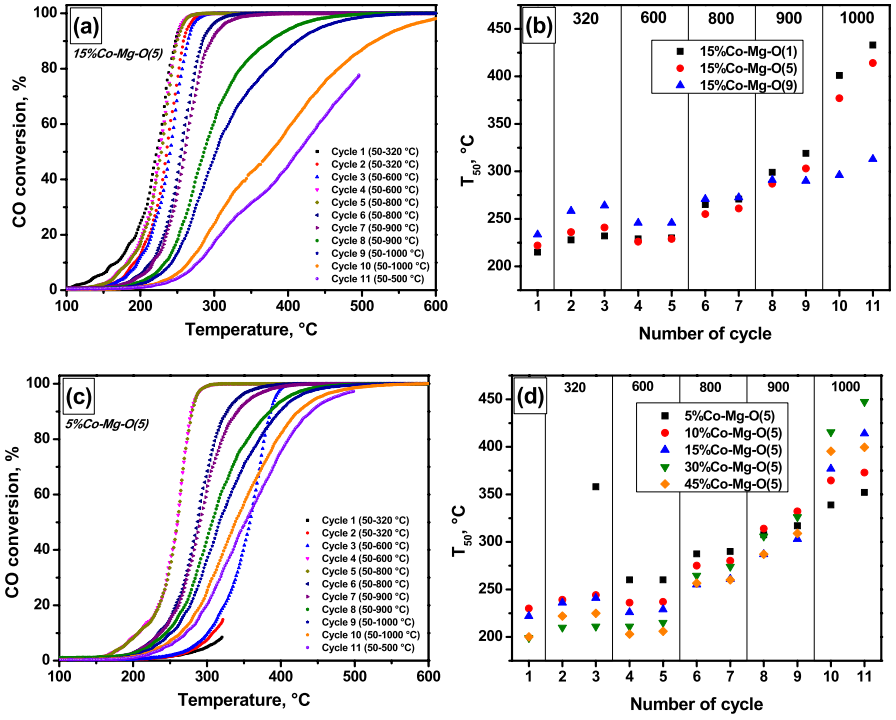

Fig. 5 Light-off curves for the 15%Co–Mg–O(5) sample (**a**). Comparison of T_{50} in catalytic cycles for the 15%Co–Mg–O samples obtained at various pH (**b**). Light-off curves for the 5%Co–Mg–O(5) sample (**c**). Comparison of T_{50} in catalytic cycles for the Co–Mg–O(5) samples with different cobalt concentrations (**d**)

samples behave similarly until the eighth cycle. The 15%Co–Mg–O(1) and 15%Co–Mg–O(5) systems exhibit slightly better catalytic performance if compared with the 15%Co–Mg–O(9) sample. As mentioned, the Co-containing species in the latter case are the smallest and strongly interacted with MgO. After the heating up to 900 °C, rapid deactivation is observed for the first two samples. At the same time, 15%Co–Mg–O(9) demonstrates remarkable stability. Such a similar behavior of the 15%Co–Mg–O(1) and 15%Co–Mg–O(5) systems is expected, taking into account the characterization results discussed above. It should be also noted that a shift of the light-off curves towards lower temperatures is evident for all the samples after the heating up to 600 °C. As already mentioned, the substitution of Co^{2+} ions with Mg^{2+} ions in the Co_3O_4 lattice can be responsible for the observed changes in catalytic performance. The formation of the solid solutions of a spinel type during the thermal treatment of CoO_x/MgO systems in an oxidative atmosphere has been also reported in the literature [52]. It is important to mention that the amount of Mg^{2+} ions in the Co_3O_4 lattice should be optimal to exhibit the best catalytic performance [12]. Further increase in the aging temperature leads to the agglomeration of the cobalt oxide particles, which affects the

catalytic properties negatively. Moreover, the aging at 900 °C changes the shape of the light-off curves (Fig. 5a). Finally, when the aging temperature reaches 1000 °C, almost complete dissolution of cobalt oxide inside the MgO matrix with the formation of solid solutions $Mg_{1-x}Co_xO$ occurs [27], and the shape of the light-off curves changes even more dramatically.

Thereby, there are two main factors affecting the catalytic activity, which are the dispersion of the active cobalt species and the textural characteristics of the MgO matrix. When the pH values are 1 and 5, the highest SSA values (119 and 165 m^2/g, accordingly) are obtained (Table 1). The 15%Co–Mg–O(9) sample is characterized by the worse SSA of 71 m^2/g. Consequently, despite the better dispersion of the cobalt species, this sample demonstrates the worst initial catalytic performance. Then, the SSA of the 15%Co–Mg–O(1) and 15%Co–Mg–O(5) samples diminishes significantly during the high-temperature aging, thus resulting in the observed rise of the T_{50} values (Fig. 5b). This process is accompanied by the movement of cobalt into the bulk of the MgO matrix and the formation of the $Mg_{1-x}Co_xO$ solid solutions. In the case of 15%Co–Mg–O(9), the changes occurred are not so dramatic.

Fig. 5c presents light-off curves for the 5%Co–Mg–O(5) sample and Fig. 5d shows the effect of cobalt loading on the catalytic behavior and stability of the prepared samples. Note that for the 5%Co–Mg–O(5) sample, 50% of CO conversion was not achieved in the first two cycles, when the final temperature did not exceed 320 °C. According to the position of light-off curves in the first runs, the samples can be ranked as follows: 5%Co–Mg–O(5) < < 10%Co–Mg–O(5) < 15%Co–Mg–O(5) < 30%Co–Mg–O(5) ≈ 45%Co–Mg–O(5). All the samples, except of 30%Co–Mg–O(5), show the reactivation effect after the heating at 600 °C, as described above. The most noticeable changes in catalytic performance are observed for the 5%Co–Mg–O(5) sample. The shift of the light-off curves after the third cycle is attributed to the reconstruction of the active sites under the action of the reaction medium [52]. Another possible reason could be that CoO_x species, which are initially located in the bulk of the as-prepared samples, move to the surface due to the high-temperature treatment. Later on, a cycle-to-cycle deactivation is observed for these samples. After aging at 1000 °C, the best catalytic performance and, therefore, better thermal stability are demonstrated by the low-loaded samples 5%Co–Mg–O(5) and 10%Co–Mg–O(5). The observed catalytic properties of the samples illustrate the decisive role of such factors as the strength of cobalt interaction with the MgO matrix, the dispersity of the cobalt species, and the porous structure of the MgO matrix.

Conclusions

In the present work, a sol–gel approach was applied to synthesize the Co–Mg–O oxide systems. Two parameters, the loading of cobalt and the pH of the hydrolyzing solution, were varied within this study. It was found that despite the appearance of the exothermic effects during the thermal decomposition of the samples prepared with addition of ammonia or nitric acid, they possess high textural properties. According to XRD, the size of the Co_3O_4 particles decreases in a row: 5.5 nm

(pH 5); 4.0 nm (pH 1); 2.5 nm (pH 9). The cyclic reduction/oxidation experiments revealed that both the pH and the cobalt content sufficiently affect the redox and catalytic properties of the Co–Mg–O catalysts. Thus, the 15%Co–Mg–O(9) sample showed the most reproducible behavior in TPR-H_2. An increase in the Co loading diminishes the hydrogen uptake and the reducibility degree, which is supposedly due to the stronger interaction of cobalt oxide with the MgO matrix and the possible formation of a solid solution ($MgCo_2O_4$). The catalytic performance was studied in the CO oxidation reaction under prompt thermal aging conditions. The best thermal stability in the consecutive catalytic cycles was observed for the 15%Co–Mg–O(9) sample characterized by the smallest particle size of Co_3O_4. An increase in the cobalt loading in a range of 5–45% enhances the catalytic behavior but worsens the thermal stability. Additionally, the reactivation effect was oversaw after aging at 600 °C for all the samples, excluding 30%Co–Mg–O(5).

Supplementary Information The online version contains supplementary material available at https://doi.org/10.1007/s11144-022-02336-1.

Acknowledgements Characterization of the samples was performed using the equipment of the Center of Collective Use "National Center of Catalysts Research".

Funding This work was supported by the Ministry of Science and Higher Education of the Russian Federation [Project No. AAAA-A21-121011390054-1].

Declarations

Conflict of interest The authors declare that they have no conflict of interest.

References

1. Letsholathebe D, Thema FT, Mphale K, Mohamed HEA, Holonga KJ, Ketlhwaafetse R, Chimidza S (2021) Optical and structural stability of Co_3O_4 nanoparticles for photocatalytic applications. Mater Today Proc 36:499–503. https://doi.org/10.1016/j.matpr.2020.05.205
2. Aadil M, Nazik G, Zulfiqar S, Shakir I, Aly Aboud MF, Agboola PO, Haider S, Warsi MF (2021) Fabrication of nickel foam supported Cu-doped Co_3O_4 nanostructures for electrochemical energy storage applications. Ceram Int 47:9225–9233. https://doi.org/10.1016/j.ceramint.2020.12.048
3. Ma J, Wei H, Liu Y, Ren X, Li Y, Wang F, Han X, Xu E, Cao X, Wang G, Ren F, Wei S (2020) Application of Co_3O_4-based materials in electrocatalytic hydrogen evolution reaction: a review. Int J Hydrogen Energy 45:21205–21220. https://doi.org/10.1016/j.ijhydene.2020.05.280
4. Zhang W, Tay HL, Lim SS, Wang Y, Zhong Z, Xu R (2010) Supported cobalt oxide on MgO: highly efficient catalysts for degradation of organic dyes in dilute solutions. Appl Catal B 95:93–99. https://doi.org/10.1016/j.apcatb.2009.12.014
5. Nyathi TM, Fadlalla MI, Fischer N, York APE, Olivier EJ, Gibson EK, Wells PP, Claeys M (2021) Support and gas environment effects on the preferential oxidation of carbon monoxide over Co_3O_4 catalysts studied in situ. Appl Catal B 297:120450. https://doi.org/10.1016/j.apcatb.2021.120450
6. Xiao B, Zhao K, Zhang L, Cai T, Zhang X, Wang Z, Yuan J, Yang L, Gao P, He D (2018) A green and facile synthesis of Co_3O_4 monolithic catalyst with enhanced total oxidation of propane performance. Catal Commun 116:1–4. https://doi.org/10.1016/j.catcom.2018.07.013
7. Fu H, Lin J, Cao S, Chen B, Huang R, Chen H, Ding T, Sun P, Luo L (2022) Enhancing the anti-K poisoning performance of Co_3O_4 catalyst for Toluene oxidation by modifying MnO_x. J Environ Chem Eng 10:107095. https://doi.org/10.1016/j.jece.2021.107095

8. Michel L, Sall S, Dintzer T, Robert C, Demange A, Caps V (2021) Graphene-supported 2D cobalt oxides for catalytic applications. Faraday Discuss 227:259–273. https://doi.org/10.1039/C9FD00110G
9. Zhu J, Kailasam K, Fischer A, Thomas A (2011) Supported cobalt oxide nanoparticles as catalyst for aerobic oxidation of alcohols in liquid phase. ACS Catal 1:342–347. https://doi.org/10.1021/cs100153a
10. Tang X, Wang J, Ma Y, Li J, Zhang X, Liu B (2021) Low-temperature and stable CO oxidation of Co_3O_4/TiO_2 monolithic catalysts. Chin Chem Lett 32:48–52. https://doi.org/10.1016/j.cclet.2020.11.008
11. Klegová A, Pacultová K, Fridrichová D, Volodarskaja A, Kovanda F, Jirátová K (2017) Cobalt oxide catalysts on commercial supports for N_2O decomposition. Chem Eng Technol 40:981–990. https://doi.org/10.1002/ceat.201600628
12. Zhang J, Hu H, Xu J, Wu G, Zeng Z (2014) N_2O decomposition over K/Na-promoted Mg/Zn-Ce-cobalt mixed oxides catalysts. J Environ Sci (China) 26:1437–1443. https://doi.org/10.1016/j.jes.2014.05.009
13. Zamudio MA, Bensaid S, Fino D, Russo N (2011) Influence of the $MgCo_2O_4$ preparation method on N_2O catalytic decomposition. Ind Eng Chem Res 50:2622–2627. https://doi.org/10.1021/ie100658w
14. Li Y, Wang X (2019) MgO modifying Al_2O_3 to load cobalt oxide for catalytic N_2O decomposition. Catal Lett 149:1856–1863. https://doi.org/10.1007/s10562-019-02789-5
15. Furusawa T, Tsutsumi A (2005) Development of cobalt catalysts for the steam reforming of naphthalene as a model compound of tar derived from biomass gasification. Appl Catal A 278:195–205. https://doi.org/10.1016/j.apcata.2004.09.034
16. El-Shobaky GA, Doheim MM, Ghozza AM, El-Boohy HA (2002) Catalytic conversion of ethanol over Co_3O_4/MgO system treated with γ-irradiation. Mater Lett 57:525–531. https://doi.org/10.1016/S0167-577X(02)00823-6
17. Wu M, Fu Y, Zhan W, Guo Y, Guo Y, Wang Y, Lu G (2017) Catalytic performance of MgO-supported co catalyst for the liquid phase oxidation of cyclohexane with molecular oxygen. Catalysts 7:155. https://doi.org/10.3390/catal7050155
18. Ghozza AM (2003) Surface and catalytic properties of the Co_3O_4/MgO system doped with Ag_2O and MoO_3. Adsorp Sci Technol 21:627–642. https://doi.org/10.1260/026361703772776411
19. Ghozza AM, El-Shobaky GA, Mokhtar M (2016) Surface and catalytic properties of the Co_3O_4/MgO system doped with Fe_2O_3. Adsorp Sci Technol 19:621–634. https://doi.org/10.1260/0263617011494448
20. Kamioka N, Ichitsubo T, Uda T, Imashuku S, Taninouchi YK, Matsubara E (2008) Synthesis of spinel-type magnesium cobalt oxide and its electrical conductivity. Mater Trans 49:824–828. https://doi.org/10.2320/matertrans.MBW200721
21. Gu S, Hsieh CT, Huq MM, Hsu JP, Ashraf Gandomi Y, Li J (2019) Preparation of $MgCo_2O_4$/graphite composites as cathode materials for magnesium-ion batteries. J Solid State Electrochem 23:1399–1407. https://doi.org/10.1007/s10008-018-04186-1
22. Kitamura N, Tanabe Y, Ishida N, Idemoto Y (2019) The atomic structure of a $MgCo_2O_4$ nanoparticle for a positive electrode of a Mg rechargeable battery. Chem Commun 55:2517–2520. https://doi.org/10.1039/C8CC09713E
23. Silambarasan M, Ramesh PS, Geetha D, Venkatachalam V (2017) A report on 1D $MgCo_2O_4$ with enhanced structural, morphological and electrochemical properties. J Mater Sci 28:6880–6888. https://doi.org/10.1007/s10854-017-6388-6
24. Wu R, Sun J, Ma X, Bao E, Du X, Xu C, Chen H (2021) Uniform $MgCo_2O_4$ porous nanoflakes and nanowires with superior electrochemical performance for asymmetric supercapacitors. J Alloys Compd 884:161087. https://doi.org/10.1016/j.jallcom.2021.161087
25. Wang H, Mi N, Sun S, Zhang W, Yao S (2021) Oxygen vacancies enhancing capacitance of $MgCo_2O_4$ for high performance asymmetric supercapacitors. J Alloys Compd 869:159294. https://doi.org/10.1016/j.jallcom.2021.159294
26. Krezhov K, Konstantinov P (1992) On the cationic distribution in $Mg_xCo_{3-x}O_4$ spinels. J Phys: Cond Matt 4:L543–L548. https://doi.org/10.1088/0953-8984/4/42/001
27. Radwan NRE, Ghozza AM, El-Shobaky GA (2003) Solid-solid interactions in Co_3O_4–MoO_3/MgO system. Thermochim Acta 398:211–221. https://doi.org/10.1016/S0040-6031(02)00369-6
28. Okamoto NL, Shimokawa K, Tanimura H, Ichitsubo T (2019) Feasible transformation of $MgCo_2O_4$ from spinel to defect rocksalt structure under electron irradiation. Scr Mater 167:26–30. https://doi.org/10.1016/j.scriptamat.2019.03.034

29. Sexton BA, Hughes AE, Turney TW (1986) An XPS and TPR study of the reduction of promoted Cobalt-Kieselguhr Fischer-Tropsch catalysts. J Catal 97:390–406. https://doi.org/10.1016/0021-9517(86)90011-4
30. Tuti S, Pepe F (2008) On the catalytic activity of cobalt oxide for the steam reforming of ethanol. Catal Lett 122:196–203. https://doi.org/10.1007/s10562-007-9370-8
31. Sadasivan S, Bellabarba RM, Tooze RP (2013) Size dependent reduction-oxidation-reduction behaviour of cobalt oxide nanocrystals. Nanoscale 5:11139–11146. https://doi.org/10.1039/c3nr02877a
32. Choya A, de Rivas B, González-Velasco JR, Gutiérrez-Ortiz JI, López-Fonseca R (2019) On the beneficial effect of MgO promoter on the performance of Co_3O_4/Al_2O_3 catalysts for combustion of dilute methane. Appl Catal A Gen 582:117099. https://doi.org/10.1016/j.apcata.2019.05.033
33. Hafizi A, Rahimpour MR, Heravi M (2019) Experimental investigation of improved calcium-based CO_2 sorbent and Co_3O_4/SiO_2 oxygen carrier for clean production of hydrogen in sorption-enhanced chemical looping reforming. Int J Hydrogen Energy 44:17863–17877. https://doi.org/10.1016/j.ijhydene.2019.05.030
34. Alalwan HA, Cwiertny DM, Grassian VH (2017) Co_3O_4 nanoparticles as oxygen carriers for chemical looping combustion: a materials characterization approach to understanding oxygen carrier performance. Chem Eng J 319:279–287. https://doi.org/10.1016/j.cej.2017.02.134
35. Idziak K, Czakiert T, Krzywanski J, Zylka A, Kozlowska M, Nowak W (2020) Safety and environmental reasons for the use of Ni-, Co-, Cu-, Mn- and Fe-based oxygen carriers in CLC/CLOU applications: an overview. Fuel 268:117245. https://doi.org/10.1016/j.fuel.2020.117245
36. Vedyagin AA, Mishakov IV, Karnaukhov TM, Krivoshapkina EF, Ilyina EV, Maksimova TA, Cherepanova SV, Krivoshapkin PV (2017) Sol-gel synthesis and characterization of two-component systems based on MgO. J SolGel Sci Technol 82:611–619. https://doi.org/10.1007/s10971-017-4321-3
37. Veselov GB, Karnaukhov TM, Bauman YI, Mishakov IV, Vedyagin AA (2020) Sol-gel-prepared Ni-Mo-Mg-O system for catalytic transformation of chlorinated organic wastes into nanostructured carbon. Materials 13:4404. https://doi.org/10.3390/ma13194404
38. Ilyina EV, Mishakov IV, Vedyagin AA (2009) Preparation of nanocrystalline $VMg(OH)_x$ and $VO_x{\cdot}MgO$ from organometallic precursors. Inorg Mater 45:1267–1270. https://doi.org/10.1134/S0020168509110144
39. Veselov GB, Karnaukhov TM, Stoyanovskii VO, Vedyagin AA (2022) Preparation of the nanostructured Ni-Mg-O oxide system by a sol-gel technique at varied pH. Nanomaterials 12:952. https://doi.org/10.3390/nano12060952
40. Vedyagin AA, Karnaukhov TM, Cherepanova SV, Stoyanovskii VO, Rogov VA, Mishakov IV (2019) Synthesis of binary Co-Mg-O oxide system and study of its behavior in reduction/oxidation cycling. Int J Hydrogen Energy 44:20690–20699. https://doi.org/10.1016/j.ijhydene.2018.05.044
41. Diao Y, Walawender WP, Sorensen CM, Klabunde KJ, Ricker T (2002) Hydrolysis of magnesium methoxide. effects of toluene on gel structure and gel chemistry. Chem Mater 14:362–368. https://doi.org/10.1021/cm010708s
42. Boehm HP, Knözinger H (1983) Nature and estimation of functional groups on solid surfaces. In: Anderson JRA, Boudart M (eds) Catalysis. Springer, Berlin, pp 39–207
43. Vedyagin AA, Volodin AM, Stoyanovskii VO, Kenzhin RM, Plyusnin PE, Shubin YV, Mishakov IV (2017) Effect of alumina phase transformation on stability of low-loaded Pd-Rh catalysts for CO oxidation. Top Catal 60:152–161. https://doi.org/10.1007/s11244-016-0726-4
44. Vedyagin AA, Stoyanovskii VO, Plyusnin PE, Shubin YV, Slavinskaya EM, Mishakov IV (2018) Effect of metal ratio in alumina-supported Pd-Rh nanoalloys on its performance in three way catalysis. J Alloys Compd 749:155–162. https://doi.org/10.1016/j.jallcom.2018.03.250
45. Bokhimi MA, Lopez T, Gomez R (1995) Crystalline structure of MgO prepared by the sol-gel technique with different hydrolysis catalysts. J Solid State Chem 115:411–415. https://doi.org/10.1006/jssc.1995.1152
46. Liotta LF, Pantaleo G, Macaluso A, di Carlo G, Deganello G (2003) CoO_x catalysts supported on alumina and alumina-baria: influence of the support on the cobalt species and their activity in NO reduction by C_3H_6 in lean conditions. Appl Catal A 245:167–177. https://doi.org/10.1016/S0926-860X(02)00652-X
47. Van de Water GA, Bezemer GL, Bergwerff JA, Versluijs-Helder M, Weckhuysen BM, de Jong KP (2006) Spatially resolved UV-Vis microspectroscopy on the preparation of alumina-supported co

Fischer-Tropsch catalysts: linking activity to co distribution and speciation. J Catal 242:287–298. https://doi.org/10.1016/j.jcat.2006.06.004
48. Solsona B, Davies TE, Garcia T, Vázquez I, Dejoz A, Taylor SH (2008) Total oxidation of propane using nanocrystalline cobalt oxide and supported cobalt oxide catalysts. Appl Catal B 84:176–184. https://doi.org/10.1016/j.apcatb.2008.03.021
49. Basąg S, Kovanda F, Piwowarska Z, Kowalczyk A, Pamin K, Chmielarz L (2017) Hydrotalcite-derived co-containing mixed metal oxide catalysts for methanol incineration : role of cobalt content, Mg/Al ratio and calcination temperature. J Therm Anal Calorim 129:1301–1311. https://doi.org/10.1007/s10973-017-6348-7
50. Pepe F, Schiavello M, Minelli G, Jacono ML (1979) Structural characterization of the ternary system cobaltous oxide-zinc oxide-magnesium oxide solid solutions. Z Phys Chem 115:7–15. https://doi.org/10.1524/zpch.1979.115.1.007
51. Moogi S, Nakka L, Potharaju SSP, Ahmed A, Farooq A, Jung SC, Rhee GH, Park YK (2021) Copper promoted Co/MgO: a stable and efficient catalyst for glycerol steam reforming. Int J Hydrogen Energy 46:18073–18084. https://doi.org/10.1016/j.ijhydene.2020.08.190
52. Ilyina EV, Mishakov IV, Vedyagin AA, Bedilo AF (2013) Aerogel method for preparation of nanocrystalline CoO_x·MgO and VO_x·MgO catalysts. J Solgel Sci Technol 68:423–428. https://doi.org/10.1007/s10971-013-3012-y

Publisher's Note Springer Nature remains neutral with regard to jurisdictional claims in published maps and institutional affiliations.

Springer Nature or its licensor (e.g. a society or other partner) holds exclusive rights to this article under a publishing agreement with the author(s) or other rightsholder(s); author self-archiving of the accepted manuscript version of this article is solely governed by the terms of such publishing agreement and applicable law.